Characterization of the immune cell infiltration landscape in head and neck squamous cell carcinoma to aid immunotherapy

Xinhai Zhang
Changhai Hospital，Naval militray medical university
Tielou Chen
Changhai Hospital, Naval military medical university
Boxin Zhang (S441566391@163.com)
Changzheng Hospital

Research

Keywords: head and neck squamous cell carcinoma; immune cell infiltrations; tumor microenvironment; Immunotherapy

Posted Date: April 23rd, 2020

DOI: https://doi.org/10.21203/rs.3.rs-23982/v1

Version of Record: A version of this preprint was published at Molecular Therapy - Nucleic Acids on December 1st, 2020. See the published version at https://doi.org/10.1016/j.omtn.2020.08.030.

Abstract

Background: The tumor microenvironment chiefly consists of tumor cells, and tumor-infiltrating immune cells admixed with the stromal component. The recent clinical trial has shown that the tumor immune cell infiltration is correlated with the sensitivity to immunotherapy and the prognosis of head and neck squamous cell carcinoma (HNSC). However, to date, the immune infiltrative landscape of HNSC has not yet been elucidated.

Methods: We proposed two computational algorithms to unravel the immune infiltration landscape of 1029 HNSC patients. The Boruta algorithm and principal component algorithms (PCA) were employed to quantify three immune cell infiltration gene subtypes categorized as per the immune cell infiltrations pattern.

Results: The high ICI score subtype was characterized by a higher tumor mutation burden (TMB) and the immune-activated signaling pathway. However, a low ICI score subtype was categorized as per the activation of immunosuppressive signaling pathways such as TGF-BETA, WNT signaling pathway, and lower TMB. Two immunotherapy cohorts confirmed patients with higher ICI score demonstrated significant therapeutic advantages and clinical benefits.

Conclusions: This demonstrated that the ICI score could serve as an effective prognostic biomarker and predictive indicator for immunotherapy. A comprehensive understanding of the HNSC immune landscape might help in tailoring immunotherapeutic strategies for different patients.

Background

Head and neck cancer rank as the sixth most common malignancies worldwide that claim around 35000 lives per year [1]. The squamous cell carcinoma is the most common pathological type of head and neck cancer [2]. Local recurrence, cervical node metastasis, and treatment failure due to resistance to conventional chemotherapy are the leading causes of death in patients with advanced head and neck squamous cell carcinoma (HNSC).

Immunotherapy activates the host’s natural defense system, which identifies and eliminates the tumor cells. It has emerged as an effective treatment with unparalleled and synergistic survival benefits in multiple cancers [3–6]. However, a major limitation of this treatment is that it benefits only a minority of patients, suggesting the urgent need for the discovery of novel therapeutic markers associated with variation in response would tailoring appropriate immunotherapy for distinct patients [3, 7].

The tumor microenvironment (TME) of HNSC includes transformed cells admixed with immune cells and stromal cellular elements [8]. Extensive research on TME has revealed a crucial role of the tumor-infiltrating immune cells in tumor dissemination, relapse, metastasis, and therapeutic response to immunotherapy [9, 10]. For instance, tumor-associated macrophages (TAM) displays multiple pro-tumor effects by secreting immunosuppressive cytokines such as IL-10, TGF-BETA, and by enhancing the TAM

density in, which is associated with unfavorable prognosis [11–13]. On the other hand, the escalated levels of tumor-infiltrating lymphocytes (TLS) such as CD4 + T cells and CD8 + T cells have been associated with improved survival-rate and response to immunotherapy [14]. TLS cells play a crucial role in response to immunotherapy as the immune checkpoint blockade activates the pre-existing TLS cells, which recognizes and eliminates the dysplastic and neoplastic cells [15, 16]. However, a response is not assured in patients with higher infiltration of TLS, which implied that although TLS is necessary, but it is insufficient in introducing clinical benefit [13, 17, 18]. The immunosuppressive cytokines secreted by TAM can impair the TLS-mediated anti-tumor effects. Moreover, the excessive infiltration of stromal components in tumors tissue can decrease the TLS trafficking into tumors [16, 17]. It elucidates that the intercellular relationships in TME are more critical than the single-cell population. So far, the expansive landscape of immune cells infiltrating the TME of HNSC has not been elucidated.

Over the past decades, advances in the next-generation sequencing technology, specifically the NGS algorithm technology, have unveiled massive biological information about HNSC tumorigenesis and metastasis [19]. In this study, we used two computational algorithms, CIBERSORT and ESTIMATE, to analyze the gene-expression profiles of bulk tumor and to acquire a comprehensive outlook about the intra-tumoral immune landscape [20, 21]. Besides, we classified the HNSC into three discrete subtypes as per the immune cell-infiltration patterns. Conclusively, in this study, we established the ICI scores to characterize the various immune landscape, which could precisely predict patient outcome and response to immunotherapy.

Materials And Methods

HNSC datasets and samples

A total of 1029 HNSC samples data was procured from five publicly available datasets: TCGA-HNSC, GSE65858, GSE41613, GSE42743, and E-MTAB-1328. The RNA-seq (FPKM value) data of TCGA-HNSC datasets were download from the UCSC Xena browser (GDC hub: https://gdc.xenahubs.net, accessed June 15, 2019). The microarray data of GSE65858, GSE41613, GSE42743, and E-MTAB-1328 datasets were downloaded from the Array Express database (www.ebi.ac.uk/arrayexpress, accessed June 15, 2019). Out of these five datasets, overall survival data for TCGA-HNSC, GSE65858, GSE42743, and GSE41613 were available. The expression profiles (FPKM values) of TCGA-HNSC were transformed into TPM (transcripts per kilobase million), which were more similar to those resulting from microarrays [22]. The *"*ComBat*"* algorithm was applied to reduce the likelihood of batch effects from non-biological technical biases between different datasets [23].

Consensus clustering for tumor-infiltrating immune cells

Infiltration levels for immune cell types in HNSC were quantified using CIBERSORT implementation in R package [21]. It was conducted by using the LM22 signature and 1000 permutations. ESTIMATE was used to evaluate the immune and stromal content (immune and stromal score) for each HNSC sample [20]. The hierarchical agglomerative clustering of HNSC was executed based on the ICI pattern of each

sample. The unsupervised clustering method used here is the “Pam” method based on Euclidean and Ward’s linkage. This procedure was performed using the “ConsensuClusterPlus” R package [24], and it was repeated 1,000 times to ensure the stability in the classification.

Differentially expressed genes (DEGs) associated with the ICI phenotype

Patients were grouped into the ICI clusters based on immune-cell infiltration to identify genes associated with the ICI patterns. DEGs among ICI subtypes were determined by significance criteria (adjusted p-value < 0.05 and absolute fold-change > 1.4) as implemented in the R package limma.

Dimension reduction and generation of ICI score

Firstly, the patients in the TCGA cohort were categorized into several groups as per the DEGs values by using unsupervised clustering. Furthermore, gene expression values that were positively correlated with the signature of the clusters were termed as the ICI gene signatures A; conversely, signature B. It was followed by dimension reduction of the ICI gene signatures A and B by employing the Boruta algorithm [25] and principal component 1 was extracted as the signature score by employing the PCA. Lastly, we applied a method similar to GGI [26] to define the ICI score of each patient: ICI score = $PC1_A$ - $PC1_B$.

Collection of somatic alteration data

The corresponding mutation data of patients in the TCGA-HNSC cohort were downloaded from the TCGA Data Portal (https://tcga-data.nci.nih.gov/tcga/). To assess the mutational burden, we counted the total numbers of non-synonymous mutations. The somatic alterations in HNSC driver genes were evaluated for the high or low ICI score. The HNSC driver genes were accessed through the “maftool” R package [27]. The top 25 driver genes with the highest alteration frequency were selected for further analysis.

Gene expression data with immunotherapy

Two independent datasets were downloaded and analyzed to determine the predictive value of the ICI score. For the IMvigor210 data set, we used a fully documented software and data package that is freely available under the Creative Commons 3.0 license and can be downloaded from http://research-pub.gene.com/IMvigor210CoreBiologies. For the TCGA-SKCM cohort, the expression profiles and related-clinical information were downloaded from the UCSC Xena browser (GDC hub: https://gdc.xenahubs.net). To determine the ICI score, we considered a total of 298 urothelial cancer cases with complete clinical information and 80 skin melanoma cases who received immunotherapy.

Statistical analyses

All statistical analyses were conducted on the GraphPad Prism version 7.0 or SPSS version 21.0 (IBM Corporation, Armonk, NY, USA) software. We performed the Kruskal–Wallis tests to compare more than two groups and the Wilcoxon test to compare two groups. The X-tile software, which iteratively tests possible cut points to select the one with the maximum rank statistic, was used to classify patients into two subtypes in each data set to reduce the computational batch effect [28]. The Kaplan–Meier plotter

was used to generate survival curves for the subgroups in each dataset. The log-rank test was used to determine the statistically significant differences. Correlations between the ICI score subgroups and somatic mutation frequency were analyzed by using the Chi-square test. The Spearman analysis was used to compute the correlation coefficient. Two-tailed *P*-values < 0.05 were considered as statistically significant.

Results

The landscape of immuno-cell infiltrating in TME of HNSC

Firstly, we performed the CIBERSORT and ESTIMATE algorithm to quantify the activity or enrichment levels of immune-cells in HNSC tumor tissue (Additional file 4: Supplementary Table 1) [20, 21]. On the basis of 1029 tumor samples with matched ICI expression profiles from meta-cohort (GSE41613, GSE42743, GSE65858, TCGA-HNSC, E-MTAB-1328), unsupervised clustering was performed using ConsesusClusterPlus package of R software to classify the HNSC patients into distinct subtypes.

We identified three independent ICI subtypes with significant survival differences (Log-rank test, *P* = 0.018; Additional file 1: Supplementary Figure S1b, Fig. 1a-b). To further clarify the intrinsic biological differences that led to distinct clinical phenotypes, we compared the immune cell composition of the tumor microenvironment (TME). Among the three main immune subtypes, the ICI cluster-A was associated with a favorable prognosis with a median survival of 2064 days. It was marked by high naïve B cells, M1 and M2 macrophages, plasma cell, memory CD4 T cells, CD8 T cells, and gamma delta T cells infiltration. The median survival time of ICI cluster-B was 1762 days, and patients in ICI cluster-B were characterized by a significantly higher density of resting dendritic cells, activated NK cells, and follicular helper T cells. The subjects in the ICI cluster-C witnessed a shorter OS (median survival 1281 days), and exhibited a significant increase in the infiltration of activated dendritic cells, activated mast cells, neutrophils, resting NK cells, memory resting CD4 + T cells, and T regulatory cells. The Kruskal-Wallis test was used to detect the significant differences between the immune cells in three distinct ICI subtypes (Fig. 1c). Additionally, the correlation coefficient heat map was generated to visualize the universal landscape of immune cell interaction in TME (Fig. 1d).

Identified immune gene subtype

To unravel the occurrence of distinct immunophenotypes, we performed differential analyses to determine the transcriptome variations among these subtypes by limma packages of R software. In the subsequent analysis, primary emphasis was laid on the TCGA-HNSC cohort, which had the most exhaustive clinical information. We performed the unsupervised clustering of 1089 DEGs (Additional file 4: Supplementary Table 2), obtained by previous differential analyses, which classified the TCGA cohort into three genomic clusters, namely gene clusters A-C (Additional file 2: Supplementary Figure S2a-b).The 588 gene signatures that were positively correlated with the gene cluster were termed as the ICI gene signature A and the rest of DEGs were named as the ICI gene signature B (Additional file 4:

Supplementary Table 3). Concurrently, in order to reduce the noise or redundant genes, we used the Boruta algorithm to perform dimension reduction in the ICI gene signature A-B [25]. The heatmap delineates the transcriptome expression profile of 276 most abundant DEGs across the genomic cluster (Fig. 2a), which were annotated by the “clusterProfiler” R package [24]. The significantly enriched biological processes are summarized in Fig. 2c-d, and the detail description is provided in the Additional file 4: Supplementary Table S4.

Furthermore, we explored the prognostic implications of the ICI gene clusters by integrating them with survival information. The analysis was performed by using the Kaplan-Meier plotter, and we found that patients in the gene cluster A had a better prognosis while patients in the gene cluster B and C had the unfavorable outcome (Log-rank test, $P = 0.0065$; Fig. 2b). Interestingly, we found that gene clusters A and C were associated with a significantly high immune score. Multiple studies have shown that the immune system may have favorable, as well as adverse outcomes, which could be exhibited in the form of pro or anti-tumor activity, as observed in our analysis [13, 16]. As depicted in Fig. 2e, we observed that the gene cluster C showed an escalated stromal component infiltration and immunosuppression-associated M2 Macrophages, and decreased dendritic cell infiltration, which was characterized as the “immune exhausted phenotype” by the previous studies [13, 29]. The gene cluster A exhibited the highest CD8 + T cell infiltration. The active immune phenotypes were characterized by the presence of plasma cells and memory activated CD4 + T cell,. Taken together, the consistency between the immune profile and prognostic profile in different gene clusters implied that our classification method is scientific and reasonable.

Construction of the ICI score

To obtain quantitative indicators of ICI landscape in HNSC patients, we used PCA to compute two aggregate scores: (1) the ICI score A from ICI signatures gene A; and (2) the ICI score B from ICI signatures gene B. The ISA and ISB of each patient in this investigation were computed as the sum of individual relevant individual scores. Finally, we acquired the prognostic signature score that was defined as the ICI score. The patients in the TCGA cohort were stratified into two groups as the high or low ICI scores by using the optimal cut-off value acquired by the X-tile software. The distribution of patients in three gene clusters is represented in Fig. 3a. We analyzed the immune activity and tolerance condition of each group in the TCGA cohort before determining the prognostic value of the ICI score in the TCGA cohort and other independent datasets. To evaluate this, firstly, we selected the CD274, CTLA4, HAVCR2, IDO1, LAG3, and PDCD1 as immune-checkpoint-relevant signatures, and CD8A, CXCL10, CXCL9, GZMA, GZMB, IFNG, PRF1, TBX2, and TNF as immune-activity-related signatures [18, 30]. We observed that most of the immune-checkpoint-relevant genes and immune-activity-relevant genes except CD274, TBX2, HAVCR2, and TNF were significantly overexpressed in the high ICI group as demonstrated by the Wilcoxon test (Fig. 3b-c). Besides, the Gene set enrichment (GSEA) analysis revealed that the WNT signaling pathway and the TGF BETA signaling pathway were significantly enriched in the low ICI score group; natural killer cell-mediated cytotoxicity, B cell receptor signaling pathway, and T cell receptor

signaling pathway were enriched in the high ICI group (Fig. 3d-e; Additional file 4: Supplementary Table S5).

The subsequent analysis involved the evaluation of the prognostic implications of the ICI scores, ICI score subgroups analysis done using the Kaplan-Meier plotter showed that the patients in the high ICI score group (median survival time 1972 days) had significantly better OS rate than the low ICI score group (median survival time 1972 days; Log-rank test, $P < 0.0001$; Fig. 3f). Moreover, the prognostic efficiency of the ICI score was validated in GSE41613 (N = 97), GSE65858 (N = 270), and the total HNSC cohort (N = 940; Log-rank test, Additional file 3: Supplementary Figure S3a-d). However, due to inadequate clinical data, we were not able to establish a statistically significant correlation in GSE42743 (N = 79). We also evaluated the effect of adjuvant therapy on the prognosis of each ICI subgroup. We found that the survival advantage in the low ICI score group was evident in the patients who received adjuvant radiotherapy (Log-rank test, Fig. 3g-h).

The correlation between the ICI score and somatic variants

A myriad of evidence has demonstrated that tumors harboring high mutation burden (non-synonymous variants) were associated with increased CD8 + T cell infiltration in tumor tissue. It facilitates the recognition and elimination of such tumors by the immune system and implies that tumor burden mutation (TMB) might determine the individual's response to cancer immunotherapy [31, 32]. An increased TMB has been correlated to an improved response to PD-1 blockades and prolonged PFS in KEYNOTE 012 clinical trial [3, 33]. Considering the significant clinical implications of TMB, we sought to explore the intrinsic correlation between the TMB and ICI scores to elucidate the genetic imprints of each ICI sub-group. To execute this, we first compared the TMB of patients with high- and low-ICI score group. As shown in Fig. 4a, patients in the high ICI score subgroup showed a significantly higher TMB than patients in the low ICI score subgroup (Wilcoxon test $P < 0.001$). Further correlation analyses confirmed that the ICI score was significantly and positively correlated with the TMB (Spearman coefficient: R = 0.1227, $P = 0.0065$; Fig. 4b). Next, we categorized the patients into discrete subgroups based on the immune set point of TMB determent by the previous study [33]. As demonstrated in Fig. 4a, we found that patients with low TMB showed better OS than the high TMB (Log-rank test, $P = 0.0667$). Taking into account the contraindicatory prognostic value of TMB and ICI score, we next evaluated the synergistic effect of these scores in prognostic stratification of HNSC. As represented in Fig. 4d, the analysis done using the Kaplan-Meier plotter revealed that the ICI score was independent of TMB (Log-rank test, HH versus LH, $P < 0.0001$; LH versus LL, $P = 0.0203$). Collectively, these findings indicate that the ICI score might serve as an underlying predictive indicator that is independent of TMB and effectively measures the response to immunotherapy.

Furthermore, we assessed the distribution of somatic variants in HNSCS driver genes between the low and high ICI subgroup. The HNSC driver genes were accessed by using the maftools [27]. The top 25 driver genes with the highest alteration frequency were selected for further analysis (Fig. 4e). Analysis of the mutation annotation files of the TCGA cohort revealed that the alteration frequency of TP53, NSD1, CSMD3, SYNE1, PKHD1L1, USH2A, PIK3CA, CASP8, FLG, PCLO, AHNAK, COL11A1, and RYR2 was

significantly different between the low and high ICI score groups (Chi-square test, Additional file 4: Supplementary Table S6). These outcomes might provide novel ideas for investigating the mechanism of tumor ICI composition and gene mutation in immune checkpoint blockade therapy.

The role of ICI scores in the prediction of immunotherapeutic benefits

Emerging immune checkpoint blocking therapy, which is used in cancer treatment to block the T cell inhibitory molecules in cancer treatment, has shown astounding outcomes with the potential in improving diseased conditions in advance cancers, but it is not effective in all the patients [3, 4]. In the subsequent analysis, we examined the utility of the ICI score in speculating the therapeutic benefit in patients. To conduct this, the patients who received anti-PD-L1 immunotherapy in the IMvigor210 cohorts were assigned the high or low ICI score groups. Notably, patients with high ICI score significantly outlived patients with low ICI scores in the IMvigor210 cohort (Log-rank test, $P = 0.0017$; Fig. 5a). The objective response rate of anti-PD-L1 therapy was higher in the high ICI score group than the low ICI group in the IMvigor210 cohort (Chi-square test, $P = 0.0143$; Fig. 5b). We also found that higher ICI scores are correlated with objective response to anti-PD-L1 therapy in the IMvigor210 cohort (Wilcoxon test, $P < 0.0001$; Fig. 5c). A similar outcome was observed in the TCGA-SKCM cohort, which received distinct immunotherapies such as cytokines, vaccines, and checkpoint blockers (Log-rank test, $P = 0.0470$, Fig. 5d; Chi-square test, $P = 0.0143$, Fig. 5e; Chi-square test, $P = 0.1520$, Fig. 5f). Collectively, these data indicate that ICI score could be correlated to response to immunotherapy.

Discussion

The early clinical trials of immunotherapy have demonstrated its high efficacy in tumorigenic growth eradication and improvement in the quality of life in patients with advanced HNSC. Due to these factors, the US Food Drug Administration and the European Medicines Agency has approved pembrolizumab as the front-line treatment in subjects with unresectable recurrent/metastatic HNSC [3]. A significant limitation of immunotherapy is that only a minority of patients are benefited from it. Even the Society for immunotherapy of Cancer who issued the first guidelines on immunotherapy for the treatment of HNSC has appealed the need to identify appropriate patients for immunotherapy [34]. In this study, we established a methodology to quantify the comprehensive tumor immune milieu of HNSC patients. The outcome of our study revealed that the ICI score is an efficient prognostic biomarker and predictive indicator in assessing the response to immunotherapy.

Mounting evidence has identified that the immune cell dysfunction within the HNSC-TME promotes immunosuppression and so the associated tumor survival and progression, which later demands therapeutic intervention to counteract this process [35, 36]. In this study, we analyzed the immune cell infiltration in a meta-cohort of 1029 HNSC samples and categorized the HNSC into three distinct immune subtypes.Our analysis indicated that density of CD4 + T cells, CD8 + T cells, plasma cells, and M1 Macrophages cells along with the higher immune score were correlated to the patient's prognosis, which

is in line with the previous studies [37, 38]. This emphasizes the fact that the pre-existing immune response has an anti-tumor effect and positively affects the response to immunotherapy. A few pioneering clinical and genomic studies [17, 20, 39] reported that HNSC is one of the most highly immune-infiltrated tumors, however, less than 20% of HNSC patients respond to immunotherapy or even lower than types of tumors with low immune infiltration. [3, 40]. This insinuates that even the immune phenotypes in the tumor cannot absolutely predict the response to immunotherapy. The molecular analysis of HNSC has identified a series of cytokines, chemokines, and other TME components that determine the host's ability to exercise anti-tumor immune response. These molecular alterations during the tumorigenesis may disturb the intercellular communication between the infiltrating immune cells, and thus tip the balance between immunity tolerance and activity [16].

In the current study, we hypothesized that the comprehensive characterization of the ICI profiles and immune-related gene expression pattern would be a novel approach in strategizing the patient-specific tailored therapy. Our primary concern was the molecular characterization of HNSC-TME that modulates the immune system, and so we first fetched the immune-related genes based on previous and present novel ICI gene clusters. Within these gene clusters, we found that ICI gene cluster B had the lowest immune score, stromal score, and other immune response-related cells, which suggests an immune-cold phenotype. Conversely, the ICI gene clusters A and C exhibited relatively high immune score and inflammatory cell density. Also, we observed that a higher stromal score enhanced the infiltration of tumor-associated macrophages and resting DCs in ICI gene clusters C, implying a humoral immune response in this cluster [29, 41]. Additionally, the ICI gene clusters A had a more favorable immune-activated phenotype with the highest density of CD8 + T cells, activated CD4 + T cells, and plasma cells [42, 43]. On the other hand, the impact of the TME on patients' overall survival was well documented by the previous studies [13, 44]. In line with these findings, our results revealed that the humoral immune response in the ICI gene clusters C and immune-cold phenotype in ICI gene clusters B was associated with a poor prognosis that could trigger tumor cell evasion from the immune system and impart resistance to immunotherapy. The anti-tumor immune response in the ICI gene clusters A was associated with favorable prognosis, and we speculated that the patients in ICI gene clusters A might likely be benefitted from immunotherapy. The outcome of our analysis is in line with the previous studies, which indicates that the gene clusters in the current study might lead to the development of more precise immunotherapy.

The individual-based model derived from tumor subtype-specific biomarkers has been well established in breast and colorectal cancer to improve outcome prediction [45, 46]. In the current study, with the help of the Boruta algorithm, we obtained potential "subtypes biomarkers" and established an ICI score to quantify the immune cell infiltration pattern. Through GSEA analysis, we found genes that were involved in the immunosuppressive pathways such as TGF-BETA and WNT signaling pathway, and these genes were enriched explicitly in the low ICI scores groups. Recently, the preclinical reports have identified an association between the gene mutations and response or tolerance to immunotherapy [47, 48]. An integrated ICI score at the genome level revealed the significant variant frequency differences in multiple genes between the high and low ICI scores, and few of these genes were explicitly associated with

sensitivity or resistance. Besides, we also detected that the TMB, which is more sensitive to immunotherapy, was significantly reduced in patients with low ICI scores. The correlation between the ICI score and TMB was found to be 0.1227. The stratified analysis revealed that the prognosis value of ICI scores was independent of TMB in HNSC. The lack of correlation, coupled with the observed individual predictive values and GSEA analysis outcome, implies that the ICI score and TMB represent distinct aspects of tumor immunobiology and can predict patient response to immunotherapy independently of TMB.

The patients receiving immunotherapy were assessed by the IMvigor210 and TCGA-SKCM, and we found that the ICI score was significantly elevated in patients responding to immunotherapy, which validated its predictive value. Overall, this suggests that single-agent immunotherapy might be beneficial in the patients with the high ICI score, whereas TGF-BETA inhibition plus immune checkpoint blockade might be beneficial in patients with low ICI scores. In this context, previous preclinical studies [49, 50] have confirmed that the synergistic therapeutic of TGF-BETA inhibitor and immune checkpoint inhibitor more efficient than the single-agent immunotherapy for solid tumors. Moreover, there is an ongoing phase-1b/2 clinical trial (NCT02423343) to test the therapeutic effects of the combined application of TGF-BETA and nivolumab in advanced solid tumors. Furthermore, the findings of the current investigation need to be validated in a larger HNSC cohort receiving immunotherapy.

Conclusions

The comprehensive analysis of tumor ICI has unraveled the mechanism by which the tumors respond to immunotherapies, which might promote the development of novel drug combination strategies for human cancers and the identification of ideal candidates for immunotherapy.

Abbreviations

HNSC: head and neck squamous cell carcinoma; PCA: principal component algorithms; TMB: tumor mutation burden; TME: tumor microenvironment; TAM: tumor-associated macrophages; TLS: tumor-infiltrating lymphocytes; TPM: transcripts per kilobase million; GSEA: Gene set enrichment analysis; DEGs: Differentially expressed genes; OS: overall survival

Declarations

Ethics approval and consent to participate

Not applicable.

Consent for publication

Not applicable.

Availability of data and materials

The gene expression data of HNSCC patients were deposited in the Array Express (www.ebi.ac.uk/arrayexpress) and UCSC Xena browser (GDC hub: https://gdc.xenahubs.net). Besides, please contact the author for data and materials requests.

Competing interests

The authors declare that they have no competing interests.

Funding

None.

Authors' contributions

Dr. B Z conceived, designed the whole project and drafted the manuscript. Prof. H Z analyzed the data and wrote the manuscript. Prof. X Z carried out data interpretations and helped data discussion. Prof. T C provided special expertise and collaboration in data analysis. All authors read and approved the final manuscript.

Acknowledgements

None.

References

1. Bray F, Ferlay J, Soerjomataram I, Siegel RL, Torre LA, Jemal A. Global cancer statistics 2018: GLOBOCAN estimates of incidence and mortality worldwide for 36 cancers in 185 countries. CA Cancer J Clin. 2018;68(6):394-424.
2. Shield KD, Ferlay J, Jemal A, Sankaranarayanan R, Chaturvedi AK, Bray F, et al. The global incidence of lip, oral cavity, and pharyngeal cancers by subsite in 2012. CA Cancer J Clin. 2017;67(1):51-64.
3. Seiwert TY, Burtness B, Mehra R, Weiss J, Berger R, Eder JP, et al. Safety and clinical activity of pembrolizumab for treatment of recurrent or metastatic squamous cell carcinoma of the head and neck (KEYNOTE-012): an open-label, multicentre, phase 1b trial. The Lancet Oncol. 2016;17(7):956-65.
4. Curran MA, Montalvo W, Yagita H, Allison JP. PD-1 and CTLA-4 combination blockade expands infiltrating T cells and reduces regulatory T and myeloid cells within B16 melanoma tumors. Proc Natl Acad Sci U S A. 2010;107(9):4275-80.
5. Garassino MC, Gadgeel S, Esteban E, Felip E, Speranza G, Domine M, et al. Patient-reported outcomes following pembrolizumab or placebo plus pemetrexed and platinum in patients with previously

untreated, metastatic, non-squamous non-small-cell lung cancer (KEYNOTE-189): a multicentre, double-blind, randomised, placebo-controlled, phase 3 trial. The Lancet Oncol. 2020;21(3):387-97.

6. Robert C, Ribas A, Wolchok JD, Hodi FS, Hamid O, Kefford R, et al. Anti-programmed-death-receptor-1 treatment with pembrolizumab in ipilimumab-refractory advanced melanoma: a randomised dose-comparison cohort of a phase 1 trial. The Lancet. 2014;384(9948):1109-17.
7. Hamid O, Robert C, Daud A, Hodi FS, Hwu WJ, Kefford R, et al. Safety and tumor responses with lambrolizumab (anti-PD-1) in melanoma. N Engl J Med. 2013;369(2):134-44.
8. Puram SV, Tirosh I, Parikh AS, Patel AP, Yizhak K, Gillespie S, et al. Single-Cell Transcriptomic Analysis of Primary and Metastatic Tumor Ecosystems in Head and Neck Cancer. Cell. 2017;171(7):1611-24.
9. Zeng D, Zhou R, Yu Y, Luo Y, Zhang J, Sun H, et al. Gene expression profiles for a prognostic immunoscore in gastric cancer. Br J Surg. 2018;105(10):1338-48.
10. Jiang Y, Zhang Q, Hu Y, Li T, Yu J, Zhao L, et al. ImmunoScore Signature: A Prognostic and Predictive Tool in Gastric Cancer. Ann Surg. 2018;267(3):504-13.
11. Noy R, Pollard JW. Tumor-associated macrophages: from mechanisms to therapy. Immunity. 2014;41(1):49-61.
12. De Palma M, Lewis CE. Macrophage regulation of tumor responses to anticancer therapies. Cancer Cell. 2013;23(3):277-86.
13. Chen YP, Wang YQ, Lv JW, Li YQ, Chua MLK, Le QT, et al. Identification and validation of novel microenvironment-based immune molecular subgroups of head and neck squamous cell carcinoma: implications for immunotherapy. Ann Oncol. 2019;30(1):68-75.
14. Vassilakopoulou M, Avgeris M, Velcheti V, Kotoula V, Rampias T, Chatzopoulos K, et al. Evaluation of PD-L1 Expression and Associated Tumor-Infiltrating Lymphocytes in Laryngeal Squamous Cell Carcinoma. Clin Cancer Res. 2016;22(3):704-13.
15. Rosenberg JE, Hoffman-Censits J, Powles T, van der Heijden MS, Balar AV, Necchi A, et al. Atezolizumab in patients with locally advanced and metastatic urothelial carcinoma who have progressed following treatment with platinum-based chemotherapy: a single-arm, multicentre, phase 2 trial. The Lancet. 2016;387(10031):1909-20.
16. Chen DS, Mellman I. Elements of cancer immunity and the cancer-immune set point. Nature. 2017;541(7637):321-30.
17. Senbabaoglu Y, Gejman RS, Winer AG, Liu M, Van Allen EM, de Velasco G, et al. Tumor immune microenvironment characterization in clear cell renal cell carcinoma identifies prognostic and immunotherapeutically relevant messenger RNA signatures. Genome Biol. 2016;17(1):231.
18. Ayers M, Lunceford J, Nebozhyn M, Murphy E, Loboda A, Kaufman DR, et al. IFN-γ–related mRNA profile predicts clinical response to PD-1 blockade. J Clin Invest. 2017;127(8):2930-40.
19. Hedberg ML, Goh G, Chiosea SI, Bauman JE, Freilino ML, Zeng Y, et al. Genetic landscape of metastatic and recurrent head and neck squamous cell carcinoma. J Clin Invest. 2016;126(1):169-80.

20. Yoshihara K, Shahmoradgoli M, Martinez E, Vegesna R, Kim H, Torres-Garcia W, et al. Inferring tumour purity and stromal and immune cell admixture from expression data. Nat Commun. 2013;4:2612.
21. Newman A, Liu C, Green M, Gentles A, Feng W, Xu Y, et al. Robust enumeration of cell subsets from tissue expression profiles. Nat Methods. 2015;12(5):453-7.
22. Wagner GP, Kin K, Lynch VJ. Measurement of mRNA abundance using RNA-seq data: RPKM measure is inconsistent among samples. Theory Biosci. 2012;131(4):281-5.
23. Johnson WE, Li C, Rabinovic A. Adjusting batch effects in microarray expression data using empirical Bayes methods. Biostatistics. 2007;8(1):118-27.
24. Yu G, Wang LG, Han Y, He QY. clusterProfiler: an R package for comparing biological themes among gene clusters. OMICS. 2012;16(5):284-7.
25. Kursa M, Rudnicki W. Feature Selection with the Boruta Package. J Stat Softw. 2010;101(4):271-285.
26. Sotiriou C, Wirapati P, Loi S, Harris A, Fox S, Smeds J, et al. Gene expression profiling in breast cancer: understanding the molecular basis of histologic grade to improve prognosis. J Natl Cancer Inst. 2006;98(4):262-72.
27. Mayakonda A, Lin DC, Assenov Y, Plass C, Koeffler HP. Maftools: efficient and comprehensive analysis of somatic variants in cancer. Genome Res. 2018;28(11):1747-56.
28. Camp R, Dolled-Filhart M, Rimm D. A New Bio-Informatics Tool for Biomarker Assessment and Outcome-Based Cut-Point Optimization. Clin Cancer Res. 2004;10(21):7252-9.
29. Biswas SK, Mantovani A. Macrophage plasticity and interaction with lymphocyte subsets: cancer as a paradigm. Nat Immunol. 2010;11(10):889-96.
30. Hugo W, Zaretsky JM, Sun L, Song C, Moreno BH, Hu-Lieskovan S, et al. Genomic and Transcriptomic Features of Response to Anti-PD-1 Therapy in Metastatic Melanoma. Cell. 2016;165(1):35-44.
31. Rizvi NA, Hellmann MD, Snyder A, Kvistborg P, Makarov V, Havel JJ, et al. Cancer immunology. Mutational landscape determines sensitivity to PD-1 blockade in non-small cell lung cancer. Sci. 2015;348(6230):124-8.
32. McGranahan N, Furness AJ, Rosenthal R, Ramskov S, Lyngaa R, Saini SK, et al. Clonal neoantigens elicit T cell immunoreactivity and sensitivity to immune checkpoint blockade. Sci. 2016;351(6280):1463-9.
33. Cristescu R, Mogg R, Ayers M, Albright A, Murphy E, Yearley J, et al. Pan-tumor genomic biomarkers for PD-1 checkpoint blockade-based immunotherapy. Science. 2018;362(6411):eaar3593.
34. Cohen EEW, Bell RB, Bifulco CB, Burtness B, Gillison ML, Harrington KJ, et al. The Society for Immunotherapy of Cancer consensus statement on immunotherapy for the treatment of squamous cell carcinoma of the head and neck (HNSCC). J Immunother Cancer. 2019;7(1):184.
35. Czystowska M, Gooding W, Szczepanski MJ, Lopez-Abaitero A, Ferris RL, Johnson JT, et al. The immune signature of CD8(+)CCR7(+) T cells in the peripheral circulation associates with disease recurrence in patients with HNSCC. Clin Cancer Res. 2013;19(4):889-99.

36. Davis RJ, Van Waes C, Allen CT. Overcoming barriers to effective immunotherapy: MDSCs, TAMs, and Tregs as mediators of the immunosuppressive microenvironment in head and neck cancer. Oral Oncol. 2016;58:59-70.
37. He Y, Jiang Z, Chen C, Wang X. Classification of triple-negative breast cancers based on Immunogenomic profiling. J Exp Clin Cancer Res. 2018;37(1):327.
38. Rooney MS, Shukla SA, Wu CJ, Getz G, Hacohen N. Molecular and genetic properties of tumors associated with local immune cytolytic activity. Cell. 2015;160(1-2):48-61.
39. Mandal R, Senbabaoglu Y, Desrichard A, Havel JJ, Dalin MG, Riaz N, et al. The head and neck cancer immune landscape and its immunotherapeutic implications. JCI Insight. 2016;1(17):e89829.
40. Yarchoan M, Hopkins A, Jaffee EM. Tumor Mutational Burden and Response Rate to PD-1 Inhibition. N Engl J Med. 2017;377(25):2500-1.
41. Probst HC, McCoy K, Okazaki T, Honjo T, van den Broek M. Resting dendritic cells induce peripheral CD8+ T cell tolerance through PD-1 and CTLA-4. Nat Immunol. 2005;6(3):280-6.
42. Hamanishi J, Mandai M, Iwasaki M, Okazaki T, Tanaka Y, Yamaguchi K, et al. Programmed cell death 1 ligand 1 and tumor-infiltrating CD8+ T lymphocytes are prognostic factors of human ovarian cancer. Proc Natl Acad Sci U S A. 2007;104(9):3360-5.
43. Hwang ML, Lukens JR, Bullock TN. Cognate memory CD4+ T cells generated with dendritic cell priming influence the expansion, trafficking, and differentiation of secondary CD8+ T cells and enhance tumor control. J Immunol. 2007;179(9):5829-38.
44. Li B, Cui Y, Nambiar DK, Sunwoo JB, Li R. The Immune Subtypes and Landscape of Squamous Cell Carcinoma. Clin Cancer Res. 2019;25(12):3528-37.
45. Callari M, Cappelletti V, D'Aiuto F, Musella V, Lembo A, Petel F, et al. Subtype-Specific Metagene-Based Prediction of Outcome after Neoadjuvant and Adjuvant Treatment in Breast Cancer. Clin Cancer Res. 2016;22(2):337-45.
46. Bramsen JB, Rasmussen MH, Ongen H, Mattesen TB, Orntoft MW, Arnadottir SS, et al. Molecular-Subtype-Specific Biomarkers Improve Prediction of Prognosis in Colorectal Cancer. Cell Rep. 2017;19(6):1268-80.
47. George S, Miao D, Demetri GD, Adeegbe D, Rodig SJ, Shukla S, et al. Loss of PTEN Is Associated with Resistance to Anti-PD-1 Checkpoint Blockade Therapy in Metastatic Uterine Leiomyosarcoma. Immunity. 2017;46(2):197-204.
48. Burr ML, Sparbier CE, Chan YC, Williamson JC, Woods K, Beavis PA, et al. CMTM6 maintains the expression of PD-L1 and regulates anti-tumour immunity. Nature. 2017;549(7670):101-5.
49. Ravi R, Noonan KA, Pham V, Bedi R, Zhavoronkov A, Ozerov IV, et al. Bifunctional immune checkpoint-targeted antibody-ligand traps that simultaneously disable TGFbeta enhance the efficacy of cancer immunotherapy. Nat Commun. 2018;9(1):741.
50. Lan Y, Zhang D, Xu C, Hance K, Marelli B, Qi J, et al. Enhanced preclinical antitumor activity of M7824, a bifunctional fusion protein simultaneously targeting PD-L1 and TGF-β. Sci Transl Med. 2018;10(424):eaan5488.

Supplementary Figure Legends

Figure S1. Overview of study design and Consensus matrixes of all HNSC samples (a) Overview of study design; (b) Consensus matrixes of all HNSC samples for each k (k = 2–5), displaying the clustering stability using 1000 iterations of hierarchical clustering.

Figure S2. Consensus clustering of TME cell infiltration in the ACRG cohort and DEGs among the ICI phenotypes (a)-(d) Consensus matrixes of TCGA-HNSC cohorts for each k (k = 2–5), displaying the clustering stability using 1000 iterations of hierarchical clustering; (e) Unsupervised clustering of 1089 DEGs among three ICI cluster groups to classify patients in TCGA-HNSC into three groups; (f) Venn diagram illustrating the number of DEGs among the three ICI clusters.

Figure S3. Prognostic value of ICI score in HNSC cohorts. (a) Kaplan–Meier curves for patients with high and low ICI scores in the GSE65858 cohort. Log-rank test P=0.002; (b) Kaplan–Meier curves for patients with high and low ICI scores in the GSE41613 cohort. Log-rank test P=0.0052; (c) Kaplan–Meier curves for patients with high and low ICI scores in the GSE42743 cohort; (d) Kaplan–Meier curves for patients with high and low ICI scores in the all HNSC cohort. Log-rank test P<0.0001.

Figures

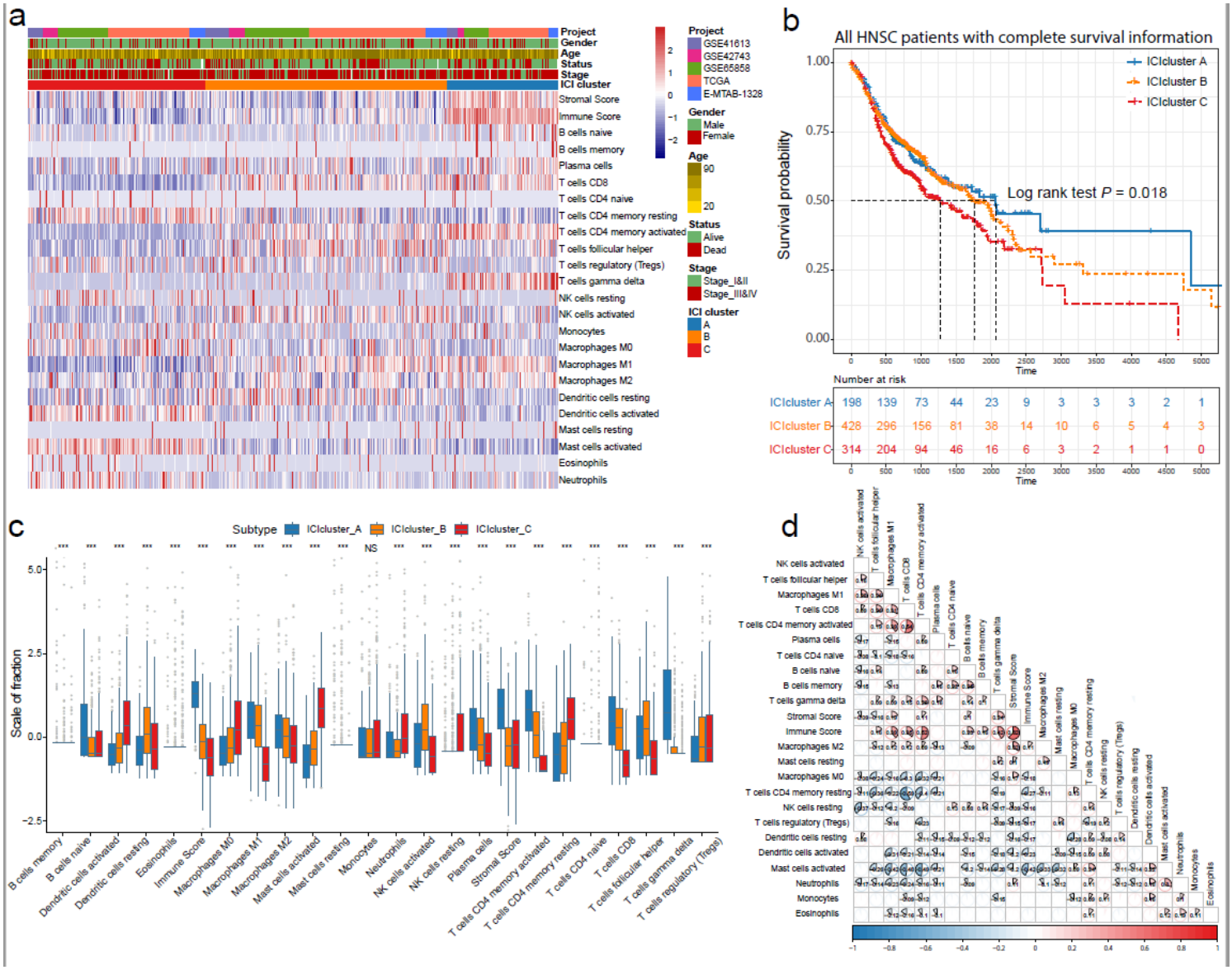

Figure 1

The landscape of immuno-cell infiltrating in TME of HNSC. (a) Unsupervised clustering of Tumor-infiltrating immune cells in five independent HNSC cohort. Rows represent Tumor-infiltrating immune cells, and columns represent samples; (b) Kaplan-Meier curves for overall survival (OS) of all HNSC patients with immune cell infiltrating classes. Log-rank test showed an overall P=0.018; (c) The fraction of Tumor-infiltrating immune cells in three ICI clusters. We also plotted the Immune score and Stromal score of three ICI clusters. The statistical difference of three ICI clusters was compared through the Kruskal-Wallis test. *, P<0.05; **, P<0.01; ***, P<0.001; ****, P<0.0001; (d) Cellular interaction of the Tumor-infiltrating immune cell types.

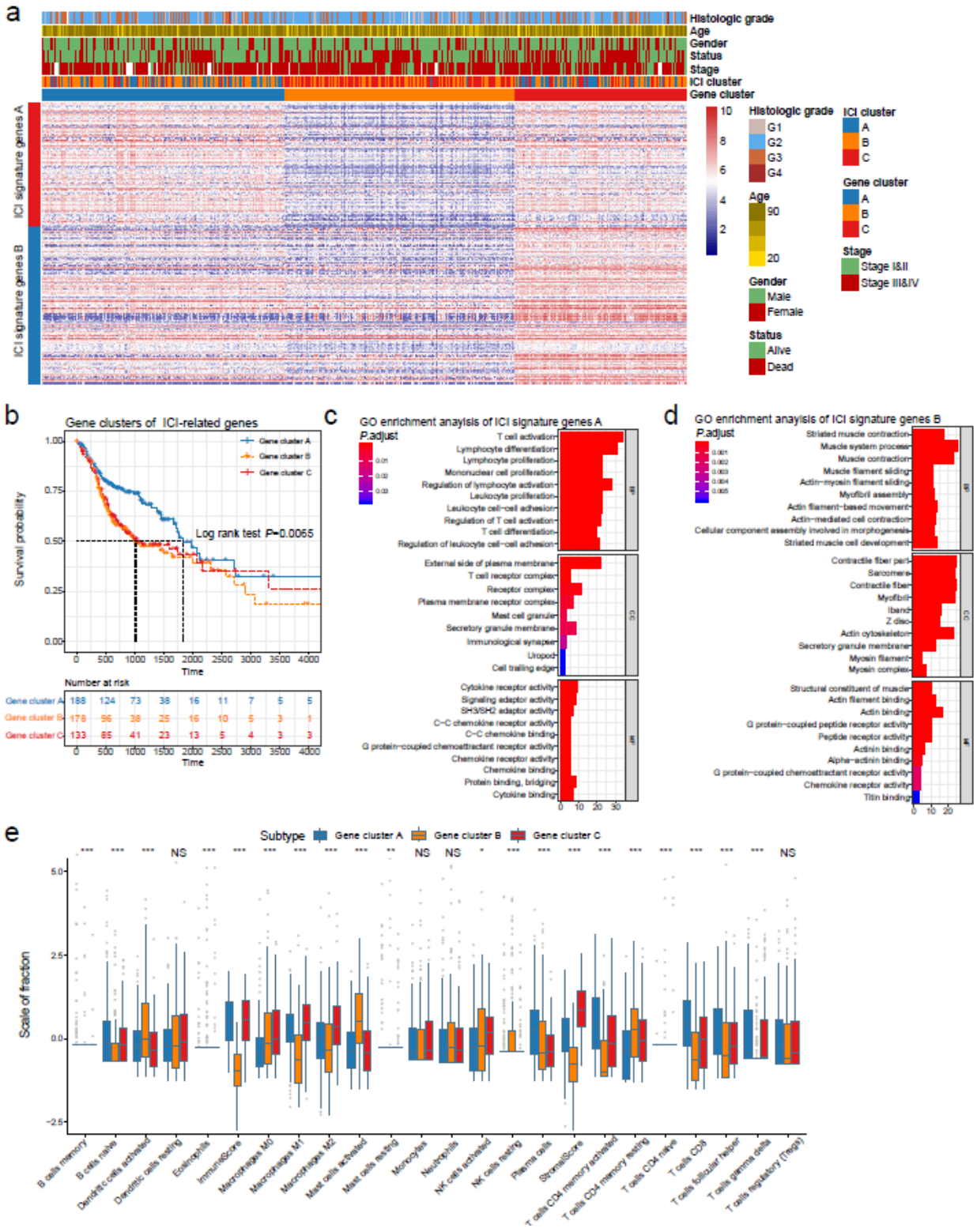

Figure 2

Identified immune gene subtype. (a) Unsupervised clustering of common DEGs among three ICI cluster groups to classify patients into three groups: Gene clusters A–C; (b) Kaplan–Meier curves for the three groups of patients. Log-rank test showed an overall P=0.0065; (c) and (d) GO enrichment analysis of the two ICI relevant signature genes—ICI signature genes (C) A and (D) B. The x-axis indicates the number of genes within each GO term; (e) The fraction of Tumor-infiltrating immune cells in three Gene clusters. We

also plotted the Immune score and Stromal score of three ICI clusters. The statistical difference of three ICI clusters was compared through the Kruskal -Wallis test. *, P<0.05; **, P<0.01; ***, P<0.001; ****, P<0.0001.

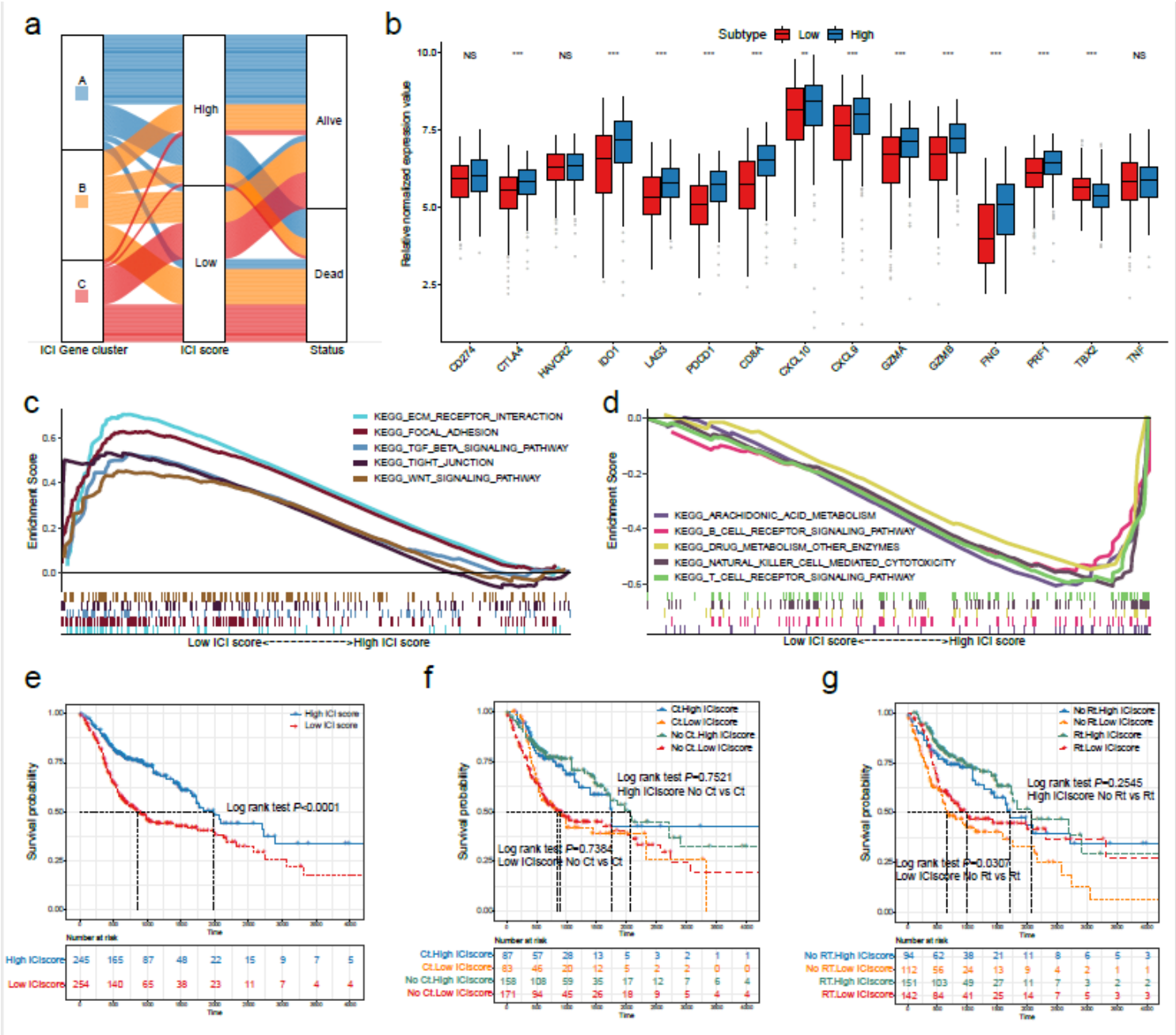

Figure 3

Construction of the ICI score (a) Alluvial diagram of ICI gene cluster distribution in groups with different ICI cluster, ICI score, and survival outcome; (b) Immune-checkpoint-relevant genes (IDO1, CD274, HAVCR2, PDCD1, CTLA4, and LAG3) and Immune activation-relevant genes (CD8A, CXCL10, CXCL9, GZMA, GZMB, PRF1, IFNG, TBX2, and TNF) expressed in high and low ICI score subgroups; (c) Enrichment plots showing Ecm receptor interaction, Focal adhesion, Tgf-beta signaling pathway, Tight junction, and Wnt signaling pathway in the Low ICI score subgroup; (d) Enrichment plots showing T cell receptor signaling pathway, B cell receptor signaling pathway, natural killer cell mediated cytotoxicity, drug metabolism other

enzymes, and arachidonic acid metabolism in the High ICI score subgroup; (e) Kaplan–Meier curves for high and low ICI score patient groups in the TCGA-HNSC cohort. Log-rank test, P<0.001; (f) Kaplan–Meier curves for patients in the TCGA-HNSC cohort stratified by both receipt of adjuvant chemotherapy (Ct) and ICI score. Log-rank test P=0.7521, High ICI score No Ct vs Ct; Log-rank test P=0.7384, Low ICI score No Ct vs Ct; (g) Kaplan–Meier curves for patients in the TCGA-HNSC cohort stratified by both receipt of adjuvant radiotherapy (Rt) and ICI score. Log-rank test P=0.2545, High ICI score No Rt vs Rt; Log-rank test P=0.0307, Low ICI score No Rt vs Rt.

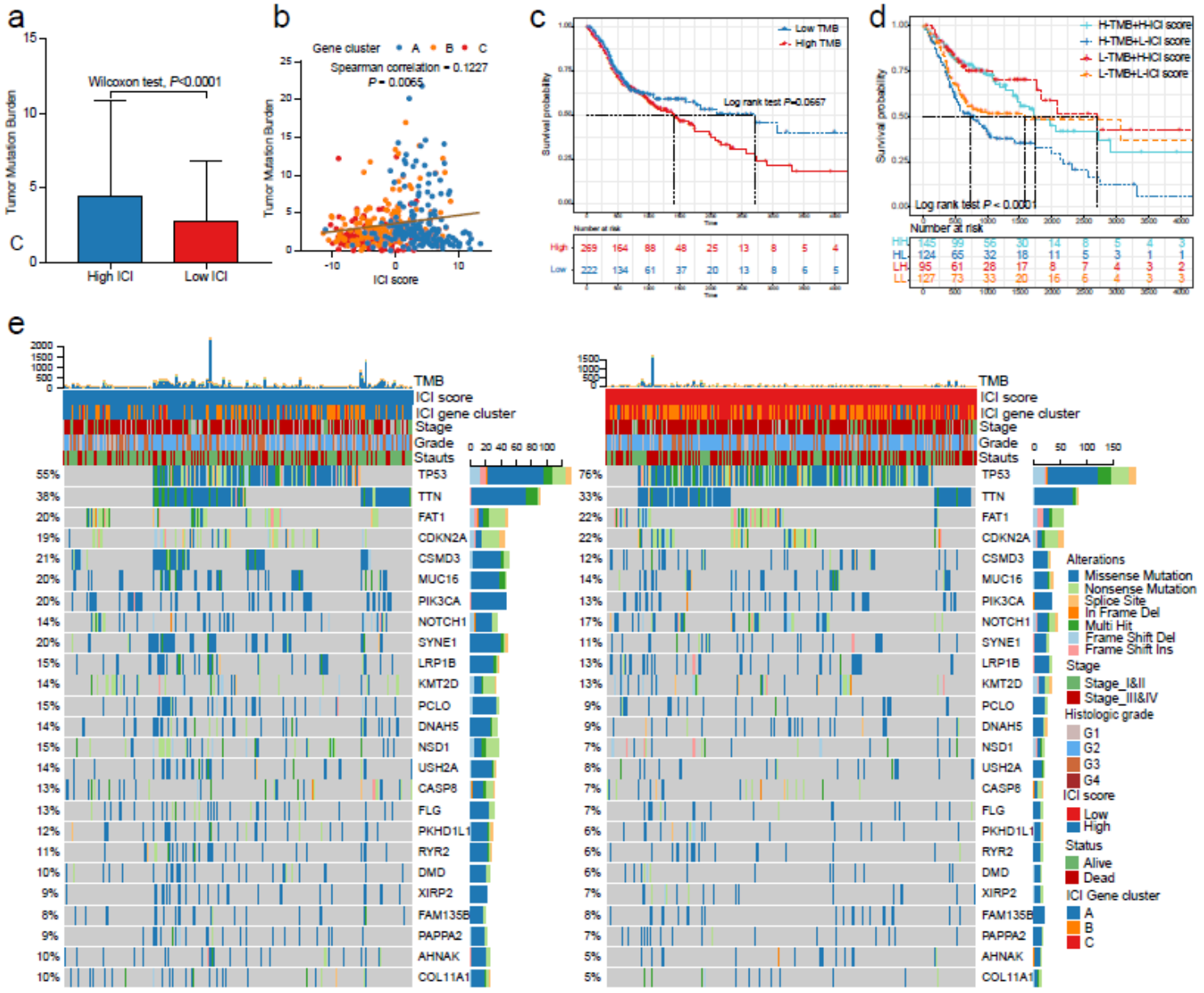

Figure 4

The correlation between the ICI score and somatic variants (a) TMB difference in the high and low ICI score subgourps. Wilcoxon test P<0.0001; (b) Scatter plots depicting the positive correlation between ICI score and mutation load in the TCGA-HNSC cohort. The Spearman correlation between ICI score and mutation load is shown (P=0.0058); (c) Kaplan–Meier curves for high and low TMB groups of the TCGA-

HNSC cohort. Log-rank test P=0.0067; (d) Kaplan–Meier curves for patients in the TCGA-HNSC cohort stratified by both TMB and ICI score. Log-rank test P<0.001. (e) The oncoPrint was constructed by those with high ICI scores on the left (red) and those with low ICI scores on the right (blue). Individual patients represented in each column.

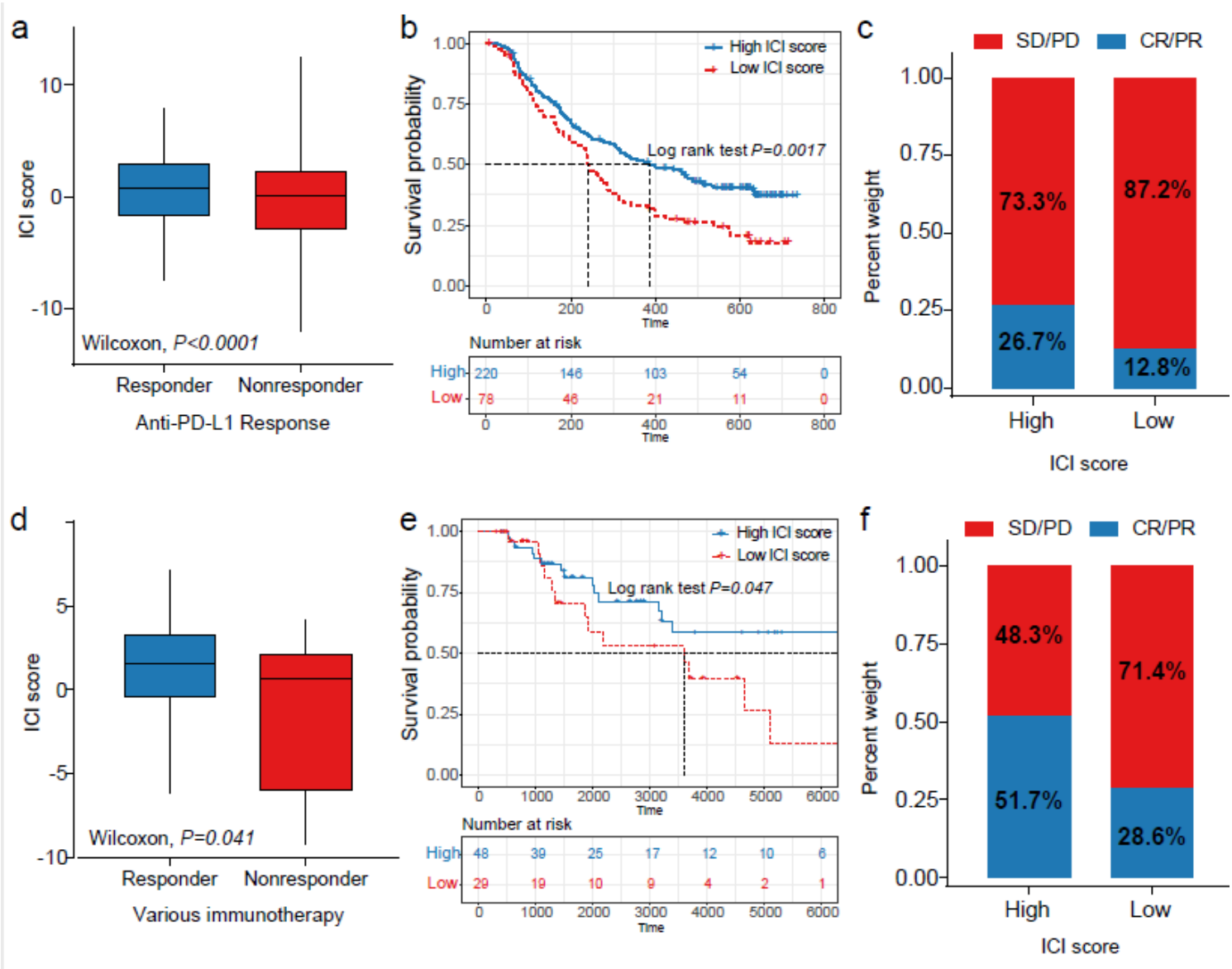

Figure 5

The role of ICI scores in the prediction of immunotherapeutic benefits (a) ICI scores in groups with different anti–PD-1 clinical response status. Wilcoxon test P<0.0001; (b) Kaplan–Meier curves for patients with high and low ICI scores in the IMvigor210 cohort. Log-rank test P=0.0017; (c) Rate of clinical response (complete response [CR]/ partial response [PR] and stable disease [SD]/ progressive disease [PD]) to anti–PD-L1 immunotherapy in high or low ICI score groups in the IMvigor210 cohort; (d). Distribution of ICI score in different response status to immunotherapy in TCGA-SKCM cohort. Wilcoxon test P=0.041; (e) Kaplan–Meier curves for patients with high and low ICI scores in the TCGA-SKCM cohort. Log-rank test P=0.047; (f) Rate of clinical response (complete response [CR]/ partial response [PR]

and stable disease [SD]/ progressive disease [PD]) to various immunotherapy in high or low ICI score groups in the TCGA-SKCM cohort.

Supplementary Files

This is a list of supplementary files associated with this preprint. Click to download.

- FigureS1.pdf
- figureS2.pdf
- SupplementaryTable.xlsx
- figureS3.pdf